



OPEN

## Synergistic effect of Ag(111) and transition metal promoters toward optimization of catalytic ethylene epoxidation selectivity

Farhad Keivanimehr, Maryam Mokhtarian & Sajjad Habibzadeh✉

The ethylene epoxidation process is crucial for selective chemical oxidation in various industrial applications. However, adding suitable promoters improves the selectivity of the commercially available Ag-catalyzed ethylene epoxidation toward ethylene oxide (EO). Empirical evidence suggests that cesium can significantly enhance the modest selectivity of silver; however, there is a need for more effective dual or multi-promoter combinations to achieve better selectivity for EO. In the present study, we employ a density functional theory (DFT) approach to investigate the impacts of Cs and various transition metal (TM) promoters—Re, Rh, Au, Cu, W, Zn, and Mo—on the ethylene epoxidation. We analyze the electronic properties of the catalysts, the adsorption energies of the reactants, and the activation barrier energies associated with the intermediates, utilizing fundamental principles and transition state theory. The results indicate that an optimal charge balance on the catalyst can be attained by combining electron-accepting TMs with electron-donating Cs. This balance effectively suppresses the formation of nucleophilic oxygen species that would otherwise improve ethylene combustion. It also mitigates the excessive electrophilicity of Ag centers, which facilitates EO isomerization. Therefore, the overall selectivity toward EO is enhanced. Indeed, the findings and methodologies presented in this work illustrate that the multi-promoted catalyst ( $\text{Ag}/\text{Cs}_{22}\text{Cu}_{24}\text{Re}_{24}\text{Au}_{30}$ ) can substantially improve the selectivity of the EO reaction, with a shift in selectivity from 1.29 to 2.71 eV when compared to the pristine Ag (111) catalyst.

**Keywords** Epoxidation of ethylene, Density functional theory, Ethylene oxide, Transition metal, Selectivity

Heterogeneous catalysts that utilize various trace promoters present a continual challenge for effective development. However, this challenge may be addressed by monitoring and predicting the influence of these promoters prior to conducting future experiments. In ethylene epoxidation, one of the most extensively investigated catalytic reactions in surface science, promoters play a vital role<sup>1–4</sup>. The resulting product from this process, ethylene oxide (EO), is an important chemical intermediate in producing several important compounds, including the ethylene glycol used in antifreeze formulations and polyester fibers. Conventionally, silver supported onto alpha-alumina has been applied as an industrial catalyst in the epoxidation of ethylene<sup>5,6</sup>. By adding Cl promoters and alkali metal additives, this catalyst has achieved over 80% EO selectivity<sup>7,8</sup>.

Numerous studies observed that the activation and adsorption of molecular oxygen are critical factors to determine EO selectivity<sup>9–12</sup>. In particular, the EO reaction is driven by adsorption, dissociation, and activation of molecular oxygen, which leads to the formation of atomic oxygen species. The ethylene adsorption and its interaction with oxygen species favor the formation of an oxometallacycle (OMC), which may be further converted to EO and acetaldehyde (AA). The latter then undergoes rapid conversion through complete oxidation to yield  $\text{CO}_2$  and  $\text{H}_2\text{O}$ <sup>13,14</sup>. This conversion is related to the formation of nucleophilic and electrophilic surface oxygen species<sup>15–18</sup>, which are responsible for nonselective total oxidation and selective epoxidation, respectively<sup>19,20</sup>.

Various promoters for Ag-based EO catalysts have been reported to modify the active oxygen species involved in the reaction. Cesium, rhenium, and chloride are well-known as effective promoters. In particular, cesium has been well investigated<sup>21–24</sup> and is believed to alter the electronic states of oxygen species adsorbed on the catalyst surface. This switching occurs through inhibiting active sites where combustion occurs, changing the transition states. This facilitates the OMC to convert more easily to EO<sup>25,26</sup> rather than to switch to AA<sup>8</sup>.

Surface Reaction and Advanced Energy Materials Laboratory, Chemical Engineering Department, Amirkabir University of Technology (Tehran Polytechnic), Tehran, Iran. ✉email: sajjad.habibzadeh@mail.mcgill.ca

Rhenium has mainly been investigated in the context of single-promoter EO catalysts<sup>27–29</sup>, yet its corresponding chemical state remains inadequately described. The electronic and geometric properties of Re promote selectivity. Specifically, the electronic influence of the Re makes the silver sites more electron-deficient<sup>30</sup>. Diao et al.<sup>30</sup> proved that Re promotes the surface oxygen species' electrophilic attack on the carbon–carbon (C–C) bond of an ethylene molecule and thus increases the selectivity of the catalyst. In addition, Re may accelerate the isomerization of the OMC intermediate to EO<sup>30,31</sup>. Conversely, EO adsorbed on Re-promoted Ag catalysts is more likely to isomerize into AA rather than desorb from the catalysts. Furthermore, the geometric effects Re are associated with the blocking of defect and step sites on Ag, which causes the adsorption and reaction of oxygen to shift toward the terraces of Ag<sup>32</sup>.

Additionally, there are limited studies on dual promoter combinations. It is important to mention that Cs-Re can be readily incorporated into an Ag-based EO catalyst, which offers much higher EO selectivity than a single Cs or Re promoter<sup>33</sup>. Özbek et al.<sup>34</sup> investigated the effect of Cl-Cs promoter combinations and realized that the main function of Cl is to occupy oxygen vacancies. They further propose considering Cl as a structural preventing agent for forming the OMC intermediate, which leads to the AA product on the oxide surface. Li et al.<sup>33</sup> applied density functional theory (DFT) simulations to explain the epoxidation of ethylene over dual-promoted Ag (110) and Ag (111) surfaces, using Cu-Re, Cs-Cu, and Cs-Re promoters. They found that Cu-Re dual-promoted surfaces have higher EO selectivity, which depends on the O-C-C angle and  $\Delta E_{ads}/d_{Ag-O}$  of OMC-type intermediate adsorbate. Chen et al.<sup>35,36</sup> also theoretically investigated ethylene epoxidation using atomic oxygen and molecular O<sub>2</sub> adsorbed on Au nanoparticles (AuNPs). They found that AuNPs possess special catalytic properties and more activity and selectivity during ethylene epoxidation. Despite recent developments in proposing new catalysts, there are few computational studies on multi-promoted surfaces at the molecular level for the C<sub>2</sub>H<sub>4</sub>/O<sub>2</sub> reaction<sup>30,33,37,38</sup>. Besides, the interaction of three or four transition metals, such as Cs-Rh, Cs-Cu-Re, Cs-Au, and Cs-Cu-Au-Re, has not been addressed in the literature. Moreover, a comprehensive study that includes the adsorption, dissociation, and reaction of reactive species on the promoted Cs-Ag catalysts by mixed transition metal oxides is lacking. Therefore, studying the C<sub>2</sub>H<sub>4</sub> oxidation mechanisms on Ag catalysts would be quite insightful, especially when transition metals (TMs) are employed in the Cs-Ag catalyst as promoters.

Likewise, the extensive theoretical and experimental research on promoters and their industrial application could not somewhat fade the respective discussions about the effect of various promoters. This is particularly important since low-content promoters are challenging to characterize accurately. Consequently, to address the limitation of previous studies, the present study aims to provide a detailed computational evaluation of the promoting effects of Cs and TM(s) on Ag-based catalysts for ethylene epoxidation. The study addresses the reactive species, the reaction mechanism, charge distribution, electronic characteristics, and the minimum energy pathway (MEP) analysis.

## Computational method

Periodic DFT calculations were conducted using the Dmol<sup>3</sup> code in the Materials Studio 7.0 software package. DFT calculations are carried out using generalized gradient approximation (GGA), as implemented by the Perdew-Burke-Ernzerhof (PBE) exchange–correlation density functional (PBE)<sup>39</sup>. Ultrasoft pseudopotentials (USP) were used, which treat all electrons explicitly but can be computationally more expensive in some cases than tabulated ultrasoft pseudopotentials. A double numeric plus polarization (DNP) was used as the basis set. Finally, empirical correction for van der Waals (vdW) interaction, according to Grimme et al.<sup>40</sup> has been considered in the calculation. For the C<sub>2</sub>H<sub>4</sub>/O<sub>2</sub> adsorption process and the ethylene oxidation reaction, the 4×4 cubic supercell was built with a slab containing up to three layers with 200 Ag atoms. Periodic boundary conditions (PBCs) were applied in the x–y–z directions to model the Ag (111) catalyst surfaces.

A 15 Å slab-slab vacuum layer was used along the z-axis to ensure sufficient repeated space between images. The unit cell parameters of the modeled supercell were chosen based on the dimensions of the Ag (111) surface and are as follows:  $a = b = 23.92$ , and  $c = 22.32$  Å;  $\alpha = \beta = 90$ , and  $\gamma = 120$  degree. Regarding geometry optimizations, a Monkhorst–Pack 5×5×1 k-point mesh was utilized to integrate over the Brillouin zone. To determine the projected density of state (PDOS), a 6×6×1 k-point was applied<sup>41</sup>. All atoms except the lowest two Ag layers were relaxed during structural optimization to an overall energy convergence at 10<sup>-6</sup> Ha (2.7×10<sup>-5</sup> eV). The global orbital cut-off, or real space cut-off, was set at 4.5 Å for all calculations. All geometry optimizations were completed with a maximum force of 0.001 Ha/Å (0.027 eV/Å) and a maximum displacement of 0.005 Å. An orbital occupation smearing of 0.005 Ha (0.136 eV) was also used to converge the electronic properties appropriately. The adsorption energy ( $\Delta E_{ads}$ ) for each adsorbate was calculated with the following equation:

$$\Delta E_{ads} = E_{total} - E_{Ag(111)} - E_{adsorbate} \quad (1)$$

where  $E_{total}$ ,  $E_{Ag(111)}$ , and  $E_{adsorbate}$  are the system's total, surface, and adsorbate energy in a vacuum, respectively.

To determine the MEP for each step in the reaction, we employed the quadratic synchronous transit (QST)/linear synchronous transit (LST) and nudged elastic band (NEB) methods<sup>42</sup>. The nature of the transition states was confirmed by analyzing vibrational frequencies, specifically looking for imaginary frequencies over the potential energy surface (PES). The simulation was halted when the orthogonal force reached 0.01 eV/Å. The highest image in the MEP was designated as the transition state (TS). For each reaction step, the activation energy barrier ( $\Delta E_{Activation}$ ) was estimated using the equation:

$$\Delta E_{Activation} = E_{TS} - E_{IS} \quad (2)$$

where IS denotes the reaction's initial state and  $\Delta\Delta E_{Activation}$  reflects the selectivity of the reaction. A larger  $\Delta\Delta E_{Activation}$  indicates higher EO selectivity, calculated as follows<sup>33</sup>:

$$\Delta\Delta E_{Activation} = \Delta E_{Activation(AA)} - \Delta E_{Activation(EO)} \quad (3)$$

where  $\Delta E_{Activation(AA)}$  and  $\Delta E_{Activation(EO)}$  are the energy barriers for  $OMC \rightarrow AA$  and  $OMC \rightarrow EO$  reactions, respectively.

In a given configuration, the binding energy is defined as<sup>13</sup>:

$$BE = E_{Ag(111)+promoter(s)} - E_{Ag(111)} - E_{promoter(s)} \quad (4)$$

where  $E_{Ag(111)+promoter(s)}$ ,  $E_{Ag(111)}$ , and  $E_{promoter(s)}$  are the energy of the promoted Ag (111), the pristine Ag (111) slab, and the promoter(s) atom, respectively. The more positive or negative binding energy indicates weaker or stronger binding.

In addition, electron density difference properties were analyzed by the CASTEP plane-wave code with USP and cut-off energy of 400 eV<sup>43</sup>.

## Results and discussion

### Structural optimization and surface models

Figure 1 presents the top and side views of optimized structures of promoted Ag catalysts. The Ag (111) surface was selected as the representative surface for the catalyst due to its superior thermodynamic stability and its prevalence in commercial EO catalysts<sup>44–46</sup>. The Ag (111) surface was modeled using a  $4 \times 4$  supercell consisting of three atomic layers of Ag. The largest species examined have an effective molecular diameter of 3.53 Å, with a center-to-center distance of 20.93 Å between two adjacent unit cells. Since every single elementary step in the reaction occurs independently on the surface of the supercell, the analysis of the reaction path itself needs to be focused entirely on those species participating in the particular action, typically two atoms or molecules. Hence, the supercell size is large enough to represent all possible relative positions among these species, with negligible impacts on the next nearest neighbor (NNN). The surface adsorbates and the upper two metal layers were allowed to relax to optimize the surface structure. For simplicity, the lower layer was constrained to the positions of bulk Ag atoms.

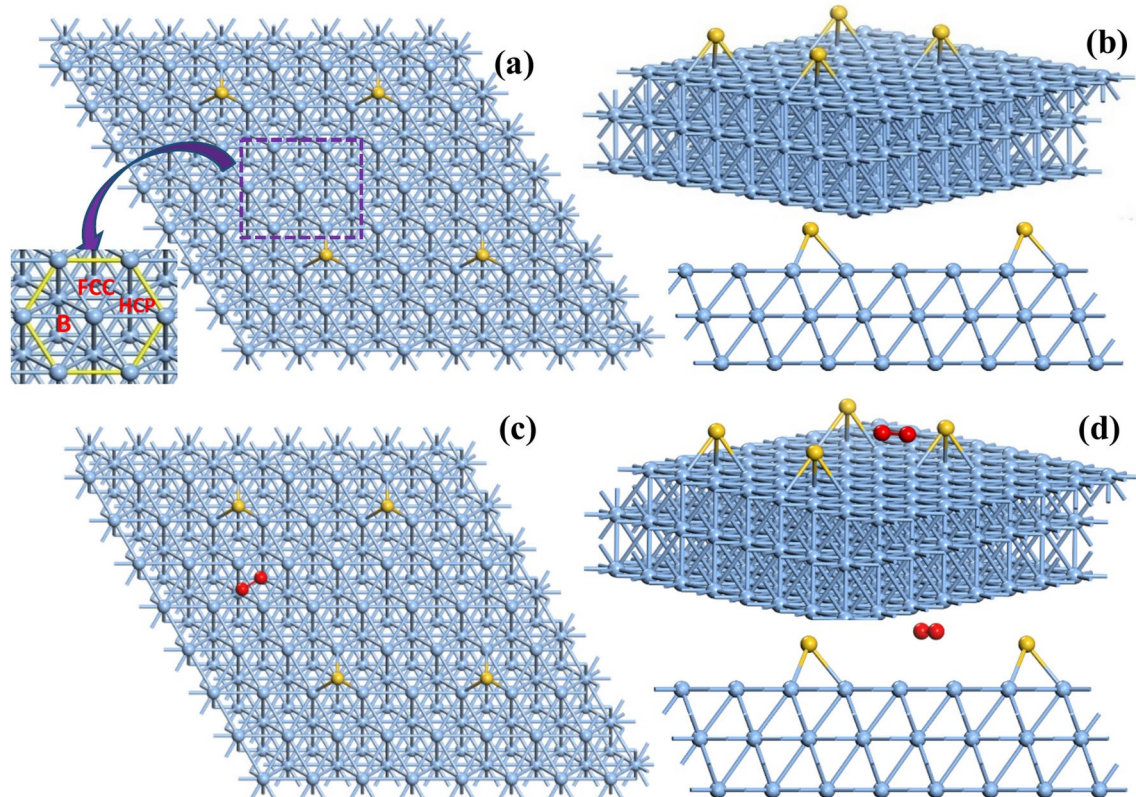


**Fig. 1.** (a) Top and (b) side views of the promoted Ag (111) catalyst. In the current model, the adsorption sites are indicated in red, while blue and yellow spheres represent the Ag and promoter(s) atoms, respectively. The adsorption sites available on the Ag (111) surface include face-centered cubic (FCC), Bridge (B), and hexagonal-close packed (HCP) configurations. (c) Top and (d) side views of the local configuration of the oxygen molecule adsorbed on the surface of the promoted Ag (111) catalyst.

Before we can look at how different promoters work together to improve the selectivity of EO during ethylene epoxidation, we need to figure out where on the Ag (111) surface each promoter is most thermodynamically optimal. In order to obtain a structure that reflects the fractional occupancy, we used the Mixture Atoms module in the Materials Studio software. By applying the Mixture Atoms module, we can simulate cases where different types of atoms occupy an atomic site. Namely, for a dual-promoter catalyst, the composition of a Cs promoter was altered to 50% Cs and 50% Au. This promoter can either bind to the surface Ag atoms as an adsorbate or become part of the surface of the Ag slab as a dopant.

In Fig. 1, the adsorption sites for the promoters (Cs, Re, Rh, Au, Cu, W, Zn, Mo, and their combination) on Ag (111) surfaces, face-centered cubic (FCC), Bridge (B), and hexagonal-close packed (HCP) are provided. Table S1 presents the adsorption energies for all the concrete promoters. The binding energy calculations reveal that the FCC site is the most favorable for the promoters to bind. The chemical bonds between the Ag and the promoter atom are formed by interactions between the d-states of the promoter and the in-plane d-states of the Ag atoms. In the optimized Ag/Cs-Au nanosheet, the metallic bonds formed between Cs-Au and three neighboring Ag atoms have a bond length of about 2.75 Å, which is much shorter than the Ag–Ag bonds of 2.91 Å in the pristine Ag (111) nanosheet, as shown in Table S1. The Ag–Ag bond lengths determined in the present study are slightly longer than the value reported by Lee et al. (2.89 Å)<sup>47</sup> and slightly shorter than that reported by Li et al. (3.10 Å)<sup>48</sup>.

Table S1 collects a summary of the BEs related to the interactions of the promoter with Ag atoms in the models developed. A lower BE value corresponds to a stronger binding affinity of the substrate to the silver. Adding either individual or mixed metal promoter moiety—regardless of their specific nature—generally results in increased substrate BEs for most systems compared to pristine Ag. Remarkably, TM dopants exhibit strong binding properties, which might account for the enhanced catalytic activity revealed experimentally<sup>31,49</sup>.

### Surface charge analysis

It is believed that nucleophilic and electrophilic oxygen atoms are responsible for both the nonselective and the selective processes<sup>50,51</sup>. Our study begins with a Hirshfeld charge analysis of oxygen at the atomic level. In the charge analysis, the oxygen atom has a significant negative charge ( $-0.390\text{ e}$ ), whereas the Ag atom has a negative net charge accumulation ( $-0.007\text{ e}$ ). The adsorbed O atom acquires a substantial number of electrons from the substrate. Consequently, the net charge accumulation on the defective Ag becomes significantly positive, from  $-0.007\text{ e}$  to  $0.034\text{ e}$ . The initial value, i.e.,  $-0.007\text{ e}$ , indicates that the silver atom featured a slightly negative charge, indicating a small excess of electrons. Also, the shift to  $0.034\text{ e}$  indicates the transition of the atom to a positively charged state, which reflects the increased positive nature of the atom's environment or a net loss of electrons.

The atomic O becomes negatively charged upon the addition of Cs, thus increasing its nucleophilic. Conversely, TMs transform that charge into a more electrophilic behavior. This is consistent with the electron-donating and electron-receiving behaviors of Cs and TMs, respectively. According to Hirshfeld charge analysis, the Re atom contributes approximately 0.26 electrons to the surface of the Ag/Cs-Re particles. In addition, due to a large amount of charge transfer, strong interactions occur between the positively charged Re and its neighbor Ag atoms. This interaction is also supported by the calculated high adsorption energy of the Cs-Re atom on the defective Ag (4.64 eV). The Cs-Re atom has a Hirshfeld charge density of 0.68 au, with the most unpaired electrons among all considered atoms. Based on the large positive atomic charge calculated, Ag/Cs-Re becomes the most active nucleophilic or radical attack site on the surface.

The Hirshfeld charge of Ag exhibits a similar pattern to that of Ag/Cs-Re, with Ag becoming more positively charged with introducing transition metal(s) and more negatively charged with adding Cs. This similarity implies that charge transfer from promoters to the catalyst surface is responsible for the Hirshfeld charge trends in atomic O and Ag. In transitional metals, electron density is accepted from silver, which subsequently interacts with atomic oxygen to increase the metal's electrophilicity. Similar coverage-dependent effects have been observed in the adsorption of O on the surfaces of various TM(s) and alloys<sup>48,52</sup>. Furthermore, donating promoter charges facilitates filling the O's p-bands and s-bands, expanding band centers. As a result, given that the p-band center of O has a broader range than the d-band center of Ag, the (O p-Ag d) band center is expected to be influenced (see Figure S4). The ionic nature of the Ag/O bond suggests that an increased O charge density improves the bonding strength of O to the surface<sup>53</sup>. In addition, nucleophilic oxygen species show considerable binding affinity to mixtures of Cs with transition metals. These results complement previous DFT studies for several such mixtures<sup>19,53</sup> and experiments<sup>27</sup>. This evidence suggests that while Cs strengthens the affinity of O, transition metals (TMSs) tend to weaken it.

### Charge density difference analysis

A charge density difference (CDD) plot was used to analyze the redistribution of electron density. Figure 2 shows the CDD of the developed catalysts, calculated by the following equation:

$$\Delta\rho = \rho_{Cat} - \rho_{Ag} - \rho_{Promoter} - \rho_O \quad (5)$$

where  $\rho_{Cat}$ ,  $\rho_{Ag}$ ,  $\rho_{Promoter}$ , and  $\rho_O$  are the charge densities of the simulated catalyst, pristine Ag (111) slab, promoter(s) atom, and pristine oxygen adsorbed systems, respectively<sup>54,55</sup>. A cutting slice, defined by the distance between the promoter atom and the nearest O atom, was oriented perpendicular to the Ag plane to illustrate the CCD. In the resulting visualization, charge accumulation and depletion by the promoters, O, and Ag atoms are presented in red and blue colors, respectively. Charge depletion is observed in most promoter atoms, except for Cs-Zn and Cs-Mo, while electron accumulation is observed repeatedly in the O atoms (Figs. 2a–o). This electron density accumulation between the O atom and the surface indicates that oxygen is polarized by the positively

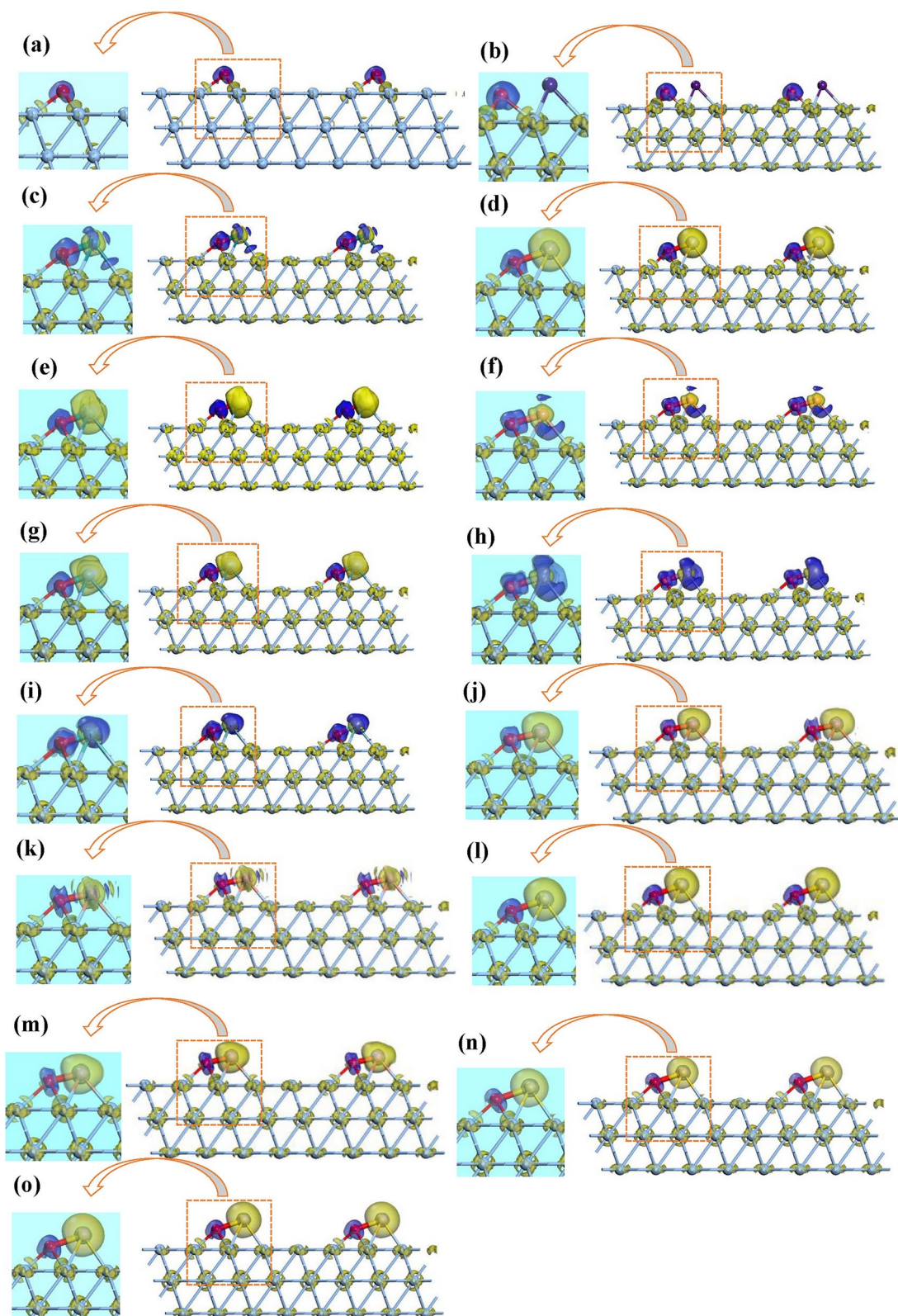


**Fig. 2.** Spatial mapping of charge density differences **(a)** Ag, **(b)** Ag/Cs, **(c)** Ag/Cs-Rh, **(d)** Ag/Cs-Au, **(e)** Ag/Cs-Re, **(f)** Ag/Cs-Cu, **(g)** Ag/Cs-W, **(h)** Ag/Cs-Zn, **(i)** Ag/Cs-Mo, **(j)** Ag/Cs<sub>33,3</sub>Au<sub>33,3</sub>Cu<sub>33,3</sub>, **(k)** Ag/Cs<sub>33,3</sub>Re<sub>33,3</sub>Cu<sub>33,3</sub>, **(l)** Ag/Cs<sub>33,3</sub>Re<sub>33,3</sub>Au<sub>33,3</sub>, **(m)** Ag/Cs<sub>25</sub>Cu<sub>25</sub>Re<sub>25</sub>Au<sub>25</sub>, **(n)** Ag/Cs<sub>22</sub>Cu<sub>24</sub>Re<sub>24</sub>Au<sub>30</sub>, **(o)** Ag/Cs<sub>22</sub>Rh<sub>24</sub>Re<sub>24</sub>Au<sub>30</sub>, catalysts. Regions of electron accumulation and depletion are denoted by blue and yellow lobes, respectively. The isosurface value of all figures is 0.08 a.u.

charged Ag atom on the surface. As previously reported<sup>56–58</sup>, the electrophilic nature of the O atom has been shown to improve EO selectivity.

Furthermore, the increased electron density surrounding the O atom results in a reduced transfer of electrons from the catalyst to the O atom, promoting the formation of electrophilic O atoms. Conversely, TM atoms enhance the electrophilic nature of O by reducing the accumulation of electron density from adjacent O atoms. This process is beneficial for producing more selective sites for ethylene epoxidation since the Cs atoms on the Ag surface increase the electron density accumulation. In addition, as shown in Fig. 2, the electronic charge density in pristine Ag (111) is spherically symmetrical around the O atoms, while that in promoted-Ag (111) catalysts is significantly asymmetrical. This kind of charge distribution is caused by factors such as valence electron delocalization or directional bonding, which substantially affects the deformation behavior of the catalysts<sup>59,60</sup>.

The findings confirm the previous hypothesis that selectivity gain is strongly connected to the promoter electric effects. In fact, previous works<sup>22,61</sup>, have reported that the promoters generate an electric field that modifies the energy of intermediates and transition states. Thus, the mixed TMs promoters, especially  $\text{Cs}_{22}\text{Cu}_{24}\text{Re}_{24}\text{Au}_{30}$  catalyst, would potentially show higher efficiency in selectivity and activity of the ethylene epoxidation reaction. This is due to the enhancement in electrophilicity of the atomic oxygen.

### Adsorption properties of molecular oxygen

The adsorbed O atom is critical in increasing EO selectivity in the ethylene epoxidation reaction process<sup>62</sup>. The active species was previously thought to be the  $\text{O}_2$  molecule<sup>25</sup>. The first stage is to characterize the adsorption of  $\text{O}_2$  molecules and O atoms on Ag surfaces, whether pristine or promoted with mixed metal. It is important to note that the ethylene epoxidation process may include a stage where molecular oxygen dissociates on the catalysts. Therefore, we investigated the adsorption of molecular oxygen as a potential starting point for the decomposition of  $\text{O}_2$ . Our study used the adsorption locator module in Materials Studio to explore various molecular oxygen adsorption configurations on the surface of the catalysts. The module suggested several configurations based on their adsorption energies. Using a systematic evaluation of multiple configurations, the most favorable configuration (i.e., the most negative adsorption value) was assigned the one with the highest adsorption energy. Following a series of studies, Table 1 summarizes the most favorable  $\text{O}_2$  adsorption configurations across various catalysts. Previous computational studies estimate that the energy released by  $\text{O}_2$  adsorption on pristine Ag varies between  $-0.243$  and  $-0.70$  eV, depending on the computational techniques, high and low oxygen coverage, and crystal size<sup>63–66</sup>. Specifically, Zhu et al.<sup>63</sup> showed an adsorption energy of  $-0.57$  eV using DFT calculations employed by PWSCF (Plane-Wave Self-Consistent Field) code in the Quantum ESPRESSO package. However, lower adsorption energy ( $-0.244$  eV) using the DMOL<sup>3</sup> code in the present study might be due to using different computational codes in calculating  $\text{O}_2$  adsorption energies. Notably, Yu et al.<sup>67</sup> reported an adsorption energy of  $-0.243$  eV for  $\text{O}_2$  on Ag (111) using the projector augmented wave (PAW) code, which closely aligns with our calculated value.

Because of the weak interaction of molecular oxygen with promoter atoms,  $\text{O}_2$  adsorption only slightly increases in mixed metal-promoted catalysts. The larger Ag– $\text{O}_2$  distance in the Cs–Ag model confirms that the Cs oxyanion plays an insignificant promotional role in dioxygen activation. Notably, the Cs atom is positioned outside the plane formed by the Ag atoms in all Cs-containing models. This arrangement is significant since it influences the interaction between the Ag and Cs atoms and their adsorption properties. This out-of-plane positioning may be influenced by the large size of the Cs atoms, although it is also important to consider the effect of the restructured surface. As depicted in Fig. 1, O atoms can occupy three possible adsorption sites on both pristine and mixed metal-promoted Ag (111) surfaces: FCC, B, and HCP. Among these, the FCC site is confirmed to be the most stable atom for O adsorption. The current study shows that Cs cannot form a covalent bond with the O atom on the Cs–Ag catalyst. The adsorption energies of the atomic oxygen at the most favorable site (i.e., FCC) on the pristine and mixed metal-promoted Ag are presented in Table 1. For instance, the calculated adsorption energy of the O atom on the pristine Ag (111) surface is  $-5.05$  eV. On the other hand, Ren et al. reported the binding energy of the O atom on the same Ag (111) surface as  $-5.92$  eV<sup>23</sup>. The differences in the observed binding energies can be attributed to the smaller size of the silver clusters, known to show unique properties compared to larger particles or surfaces, including increased reactivity<sup>68</sup>.

The mixed metal-promoted models show higher binding energies for most of the interactions investigated<sup>69–72</sup>. Notably, when Cs and Rh moieties are combined, the binding energies of atomic oxygen are significantly increased compared to the pristine Ag model. In the Ag/Cs-Rh catalyst, the energy values associated with substrate bonding with the surface are doomed “optimal,” aligning with the experimentally observed superior performance of Ag catalysts co-promoted by Rh and Cs when compared to those promoted individually by either Rh or Cs. This observation indicates the synergistic effect of the Rh and Cs promoters. Furthermore, this enhancement suggests an increase in the strength of facet-dependent adsorption. It has been demonstrated that the adsorption energy of the adsorbate on these catalysts is proportional to the d-band center (ed) of the occupied d-d-band (see Figure S4)<sup>73,74</sup>.

The results for  $\text{O}_2$  adsorption are also in acceptable agreement with those reported by Zhu et al.<sup>63</sup>, where the atomic oxygen binding energy results are similar to those obtained by Ren et al.<sup>23</sup>. The Ag–O bond length for O atom binding is consistent with the value calculated by Zhu et al.<sup>63</sup> for Ag (111) FCC sites. Notably, the Ag–O bond values indicate that the strength of the O atom is significantly greater on mixed metal-promoted Ag catalysts than on pristine Ag, as shown in Table S1. According to Table 1, the adsorption energy of the O atom on the  $\text{Cs}_{25}\text{Cu}_{25}\text{Re}_{25}\text{Au}_{25}$ -promoted Ag (111) surface increases to  $-7.77$  eV, compared to  $-5.05$  eV on the pristine Ag (111) surface.

Catalyst	Adsorption Energy per O <sub>2</sub> molecule (eV)	Configuration	Length Ag-O2	Adsorption Energy per one O (eV)	Length Ag-O
Ag	-0.244		4.494	-5.05	2.147
Cs	-0.247		3.543	-6.16	2.199
Cs-Rh	-0.249		5.238	-4.58	2.279
Cs-Au	-0.245		3.169	-5.65	2.280
Cs-Re	-0.245		3.170	-7.49	2.236
Cs-Cu	-0.245		3.183	-7.70	2.272
Cs-W	-0.250		3.151	-8.94	2.27
Cs-Zn	-0.251		3.113	-8.07	2.314
Cs-Mo	-0.249		3.153	-8.08	2.193
Cs <sub>33.33</sub> Au <sub>33.33</sub> Cu <sub>33.33</sub>	-0.245		3.2	-7.79	2.344
Cs <sub>33.33</sub> Re <sub>33.33</sub> Cu <sub>33.33</sub>	-0.246		3.205	-7.80	2.345
Cs <sub>33.33</sub> Re <sub>33.33</sub> Au <sub>33.33</sub>	-0.245		3.169	-5.65	2.294
Cs <sub>25</sub> Cu <sub>25</sub> Re <sub>25</sub> Au <sub>25</sub>	-0.245		3.183	-7.77	2.343

Continued

Catalyst	Adsorption Energy per O <sub>2</sub> molecule (eV)	Configuration	Length Ag-O <sub>2</sub>	Adsorption Energy per one O (eV)	Length Ag-O
Cs <sub>22</sub> Cu <sub>24</sub> Re <sub>24</sub> Au <sub>30</sub>	-0.248		3.195	-5.65	2.292
Cs <sub>22</sub> Rh <sub>24</sub> Re <sub>24</sub> Au <sub>30</sub>	-0.245		3.169	-5.66	2.295

**Table 1.** Calculated adsorption energies of molecular oxygen (in eV), Ag-O<sub>2</sub> bond length (in Å), and local configuration of the molecular oxygen adsorption on the promoted and unpromoted surfaces.

### Adsorption properties of ethylene

The adsorption of C<sub>2</sub>H<sub>4</sub> and O atoms on the surfaces of the developed catalysts has been calculated to gain a deeper understanding of the reaction mechanism on both pristine and mixed metal-promoted Ag surfaces. Table 2 summarizes the optimized stable structures and adsorption energies of ethylene on these Ag (111) surfaces. Tables S2, S3, and S5 indicate the presence of atomic oxygen species on the entire surface, at different positions of Ag atoms, and coordinates of O-adsorbed on the Ag/Cs-Au surface simultaneously. In addition, the atomic or lattice oxygen occupying the FCC positions acts as the active site for ethylene adsorption. The optimized geometrical parameters of ethylene are compared quite well with the theoretical values reported by Bocquet and Loffreda<sup>75,76</sup>. For example, the C-H and C-C bond lengths were found to be 1.09 Å and 1.34 Å, respectively, while the angles H-C-C and H-C-H were to be 121° and 117°. In our model, the calculated values for these parameters are 121.9° and 116.3°.

As shown in Table 2, atomic oxygen species are located on top of coordinatively unsaturated (CU) Ag atoms. All Ag<sub>cu</sub> sites can be fully covered with atomic oxygen by exposing the Ag (111) surface to multiple Langmuirs of molecular oxygen at various temperatures and oxygen pressures<sup>77,78</sup>. However, experimental evidence demonstrates that ethylene adsorption requires an empty Ag<sub>cu</sub> site. Without an empty Ag<sub>cu</sub> site, ethylene cannot bind atop the oxygen atoms<sup>78</sup>. To evaluate the current state of the ethylene epoxidation reaction, an ethylene gas molecule was positioned over the oxygen atoms to assess binding. According to calculations of these configurations, the ethylene molecule adsorbs at oxygen atom sites. The binding distance of ethylene to the Ag atom on the surface of a pristine Ag catalyst is measured at 3.71 Å.

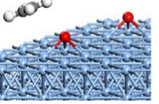
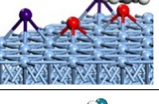
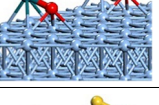
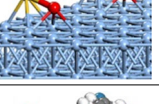
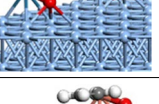
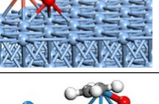
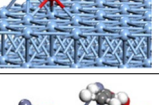
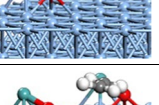
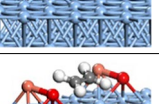
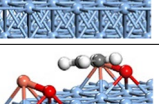
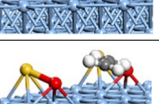
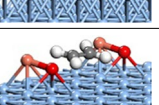
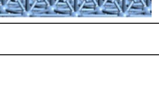
Furthermore, ethylene aligns nearly parallel to the nanosheet surface, attributed to a favorable orbital interaction between its *d* orbital and the *d* orbital of the nanosheet surface. C<sub>2</sub>H<sub>4</sub> has an adsorption energy of -0.082 eV on pristine Ag surfaces (111). According to Gao et al.<sup>79</sup>, ethylene adsorbed at a rate of -0.119 eV onto Ag sites. The differences in binding energies can be explained by the small size of the silver clusters, which are known to possess unique properties compared to larger particles or surfaces, including enhanced reactivity<sup>68</sup>. As shown in Table 2, the adsorption of C<sub>2</sub>H<sub>4</sub> on mixed metal-promoted Ag (111) surfaces shows greater stability than on pristine Ag (111) surfaces. Figure 3 illustrates the adsorption strength of C<sub>2</sub>H<sub>4</sub> on Ag (111) surfaces, indicating that the promoters exert a facet-dependent effect on the adsorption strength of the ethylene.

### Reaction mechanism of ethylene epoxidation

The conversion of C<sub>2</sub>H<sub>4</sub> to EO is depicted in Fig. 4 as a two-dimensional structural process. The minimum energy pathway for the reaction is also shown in Fig. 5, which includes the optimized structures of the reactant, transition state (TS), product structures, and relative energies. The reaction consists of ten fundamental steps, summarized and organized in Table 3. Firstly, ethylene and molecular oxygen are weakly adsorbed onto the silver surface (steps 1 and 2). The dissociative adsorption of the adsorbed molecular or gaseous oxygen generates atomic oxygen on the surface (steps 3\* and 3). There are two potential scenarios in step 4: co-adsorption of oxygen and ethylene (step 4\*) or ethylene adsorption occurring through an Eley–Rideal mechanism (step 4). Following the OMC intermediate, the reaction continues through two competing pathways previously observed on other surfaces<sup>80,81</sup>.

The first pathway builds up an epoxy ring on the Ag surface by breaking the C=C bond to form an EO molecule (step 5). This elementary reaction is exothermic, while its reaction energy of -0.63 eV indicates it may occur under typical conditions. The conversion of EO to AA through isomerization is illustrated in Fig. 4 (Step 6). Because of the strong chemical interaction between the C and the displaced H atoms, this reaction is more exothermic than the previous step, but it has a higher activation energy barrier of 1.06 eV. When assessing the degree of rate control, these processes are identified as rate-determining and selectivity-controlling<sup>82</sup>. The subsequent desorption of EO and AA molecules into the gas phase after OMC isomerization does not require a transition state and involves negligible reaction energy (steps 7 and 8). The competitive oxidation reaction to AA immediately turns into H<sub>2</sub>O, and CO<sub>2</sub> is thermodynamically favorable because  $\Delta G = -194 \text{ kJ.mol}^{-1}$ <sup>61</sup>. In other words, the energy barrier for transforming AA to CO<sub>2</sub> and H<sub>2</sub>O is much lower than that for OMC to AA. Therefore, it is reasonable to conclude that the complete combustion reaction is not a rate-determinate step in the EO reaction.

According to Jankowiak and Bartea<sup>83</sup>, the activation energy barrier for ethylene epoxidation is 0.58 eV, which is in acceptable agreement with our 0.66 eV on pristine Ag (111), considering the bulk metallic catalyst

Catalyst	Adsorption Energy C <sub>2</sub> H <sub>4</sub> (eV)	Configuration	Length O-C
Ag	-0.082		3.51
Cs	-0.102		3.667
Cs-Rh	-0.092		3.592
Cs-Au	-0.097		3.657
Cs-Re	-0.093		3.587
Cs-Cu	-0.094		3.625
Cs-W	-0.096		3.931
Cs-Zn	-0.092		3.571
Cs-Mo	-0.093		3.585
Cs <sub>33.3</sub> Au <sub>33.3</sub> Cu <sub>33.3</sub>	-0.087		3.481
Cs <sub>33.3</sub> Re <sub>33.3</sub> Cu <sub>33.3</sub>	-0.094		3.623
Cs <sub>33.3</sub> Re <sub>33.3</sub> Au <sub>33.3</sub>	-0.091		3.547
Cs <sub>25</sub> Cu <sub>25</sub> Re <sub>25</sub> Au <sub>25</sub>	-0.088		3.547

Continued

Catalyst	Adsorption Energy C <sub>2</sub> H <sub>4</sub> (eV)	Configuration	Length O-C
Cs <sub>22</sub> Cu <sub>24</sub> Re <sub>24</sub> Au <sub>30</sub>	-0.098		3.612
Cs <sub>22</sub> Rh <sub>24</sub> Re <sub>24</sub> Au <sub>30</sub>	-0.089		3.686

**Table 2.** Calculated adsorption energies of molecular oxygen (in eV), O-C bond length (in Å), and local configuration of the ethylene adsorption on the promoted and unpromoted surfaces.

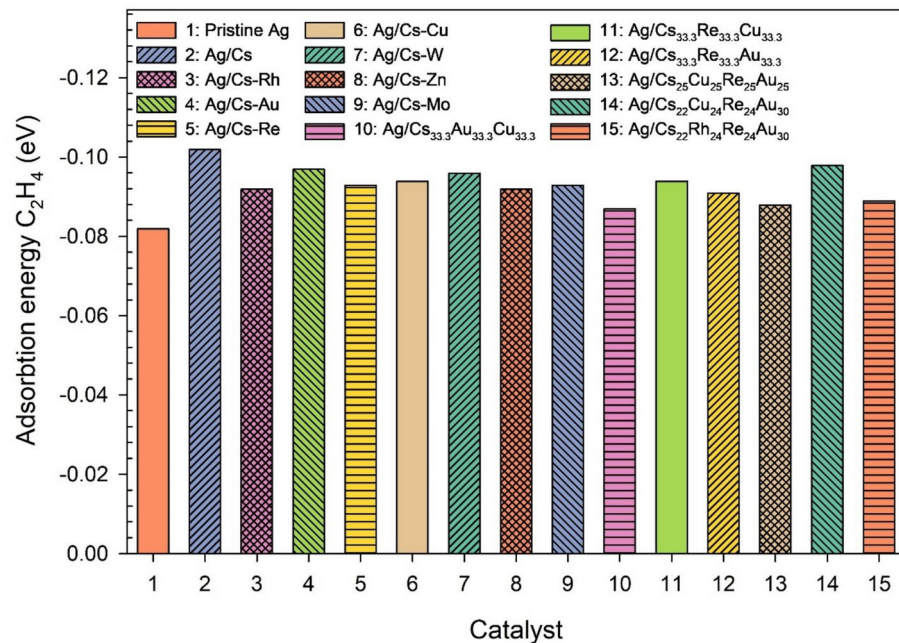


**Fig. 3.** Adsorption strength of C<sub>2</sub>H<sub>4</sub> on the promoted and unpromoted Ag (111) surfaces.

is primarily composed of Ag (111). Grant and Lambert<sup>84</sup> represented that the activation energy barriers for the mixture of C<sub>2</sub>H<sub>4</sub> and O<sub>2</sub> in a 1:1 ratio range between 0.45–0.53 eV and 0.52–0.63 eV, respectively, which are within our simulated results. Previous studies have also indicated that activation energy barriers can range between 0.4 and 1.1 eV, depending on experimental conditions and laboratory setups<sup>85,86</sup>.

This work does not include a complete oxide phase because, in general, metal oxides have a lower affinity for oxygen than metals, resulting in dramatically different scaling relationships<sup>87,88</sup>. Therefore, the present study concentrates on the general features of ethylene oxidation for small oxygen coverages. Previous computations of the O-Ag phase diagram as a function of pressure and temperature<sup>89</sup> revealed that under typical experimental conditions for ethylene epoxidation—characterized by low O<sub>2</sub> pressure (0.1 bar) and high temperatures (230 °C)—a low O-coverage on Ag (111) is thermodynamically beneficial. Furthermore, previous studies on the Ag phase diagram confirm that under the reaction conditions for ethylene epoxidation, the Ag<sub>2</sub>O surface is unstable. In fact, the Ag surface partially oxidized during the reaction<sup>45,46,90</sup>.

Moreover, prior investigations that employed first principles-aided thermodynamic modeling to study the phase diagrams of the TMs in the oxygen environment (Ag<sup>89</sup>, Au<sup>91</sup>, Pt<sup>92</sup>, Cu<sup>93</sup>, Pd<sup>94</sup>, Ir<sup>95</sup>, Ni<sup>96</sup>, Ru<sup>97</sup>, Rh<sup>98</sup>) indicate that Pt and Au promoters maintain their metallic phase during ethylene epoxidation. In contrast, the promoters Ni, Cu, Ir, Pd, Ru, and Rh fully change to their corresponding oxide states. According to XPS spectra, Diago et al. show that Re and Mo oxidize in a pure oxygen environment, turning into Re<sub>2</sub>O<sub>7</sub> and MoO<sub>3</sub> phases, respectively. However, it should be noted that in real conditions of the ethylene epoxidation reaction, the oxygen concentration is about 20%, suggesting that these promoters may not be fully oxidized. Thus, based on the partially oxidized Ag surface, our present models could be relevant to the mechanism of EO production under low-pressure oxygen conditions.

To determine which catalysts are more active toward producing either ethylene oxides (EOs) or acetaldehydes (AAs), investigations into the transition state (TS) features of the two competing processes must be pursued. Figure 5 depicts the TS values for both EO and AA after OMC isomerization. The top and side views of OMC,

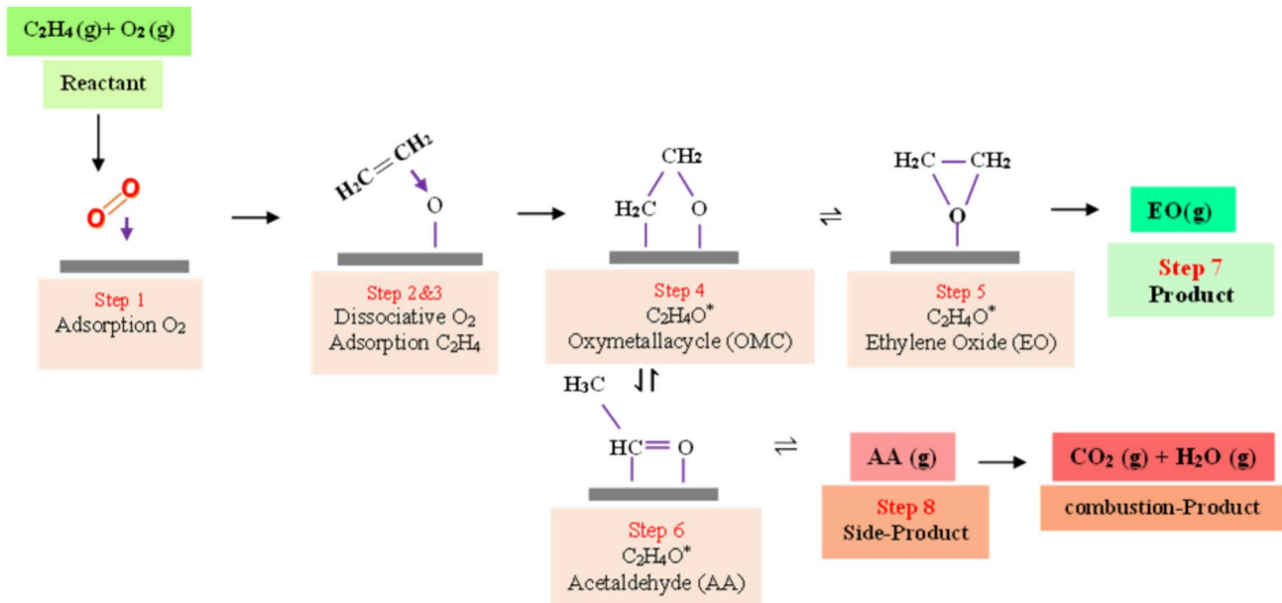


**Fig. 4.** The possible reaction mechanism for epoxidation of ethylene over the silver surface to produce EO.

EO, and AA formation over-developed catalysts are presented simultaneously in Figures S1–S3. Moreover, the highest occupied molecular orbital (HOMO) and the lowest unoccupied molecular orbital (LUMO) of specious are shown in Figure S5 and Table S4. A crystal-clear distinction is observed in the two TSs. In EO formation, the TS includes the breaking of the  $\text{C}=\text{C}$  bond to allow the epoxy ring closure. During this process, oxygen shifts beneath the ethylene fragment while the  $\text{O}-\text{metal}$  bond remains intact. On the other hand, the TS for producing AA involves the dissolution of both  $\text{C}-\text{metal}$  and  $\text{O}-\text{metal}$  bonds with the migration of H from one C atom to another, where a  $\text{C}=\text{O}$  bond is formed. These configuration properties at the two TSs are consistent across all TMs and metal oxide surfaces evaluated in this study. Experimental results indicate that the promoted and unpromoted catalysts produce significantly different amounts of EO. For instance, the activation energy barrier for EO formation is lower on an Ag surface that has been promoted with Cs-Re than a pristine Ag surface (see Fig. 5). Consequently, AA generation on a pristine Ag (111) surface is more efficient than on an Ag (111) surface enhanced with Cs-Re.

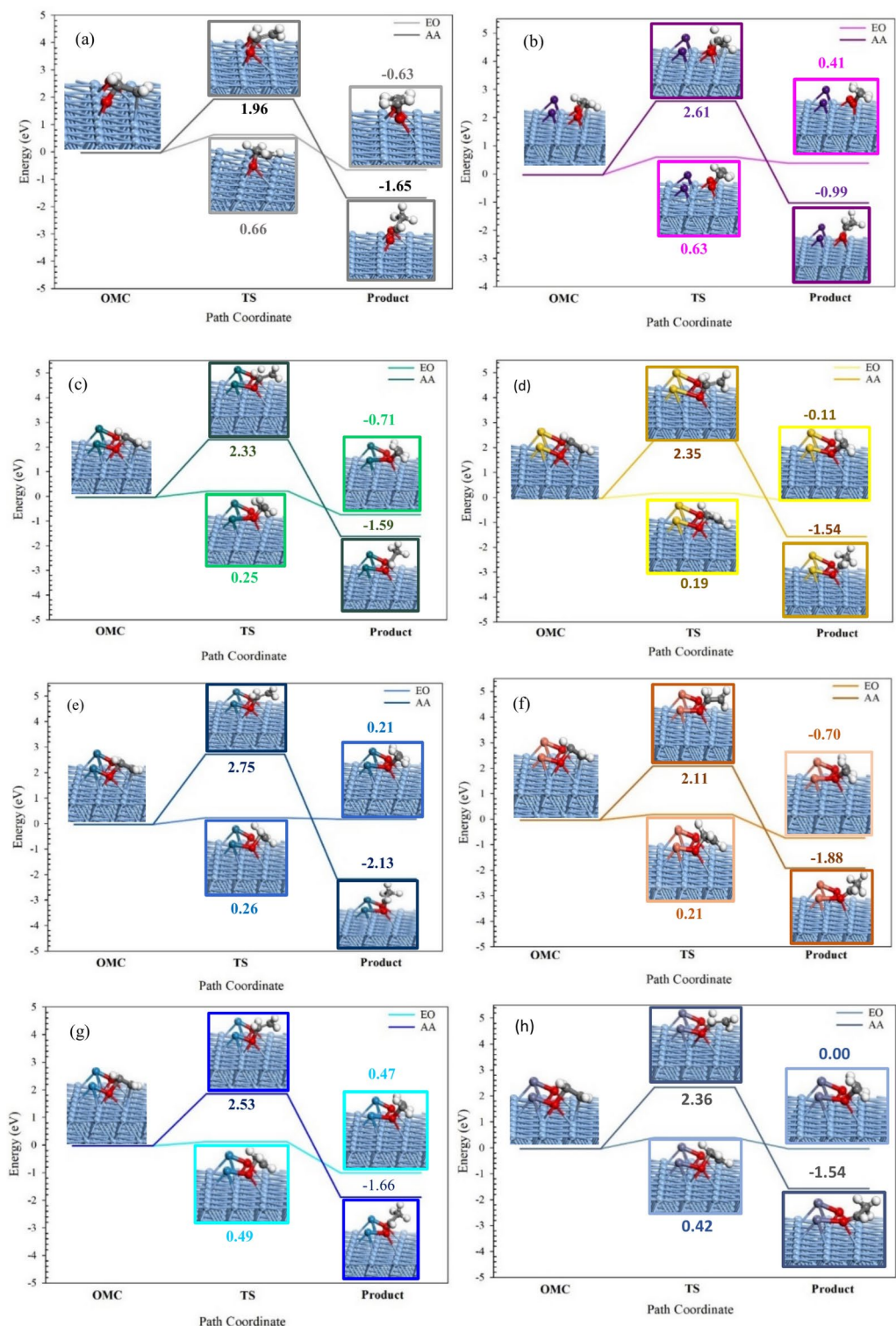
### Catalytic activity and selectivity toward EO product

Figure 5 illustrates the use of the MEP diagram of both promoted and unpromoted Ag (111) surfaces to compute their theoretical selectivity ( $\Delta\Delta E_{Activation}$ ) for EO (see Fig. 6). The  $\Delta\Delta E_{Activation}$  on the promoted Ag (111) surface, as shown in Fig. 6, is lower than that of  $\Delta\Delta E_{Activation}$  on a pristine Ag (111) surface. Further details are provided in the text. Previous reports showed that EO selectivity is greater on promoted Ag (111) surfaces than on pristine Ag (111) surfaces<sup>99,100</sup>. The activation energy barriers of the OMC intermediate to EO are lower on promoted Ag (111) surfaces, indicating that this surface is more prone to isomerization. In contrast, the activation energy barrier for isomerization of OMC intermediate into AA is higher on promoted Ag (111) than a pristine Ag (111) surface. Thus, in terms of selectivity and catalytic activity, the promoted Ag (111) surface outperforms the pristine Ag (111) surface (see Fig. 6). As a result, the selectivity and catalytic activity for EO on the promoted Ag (111) surface are much higher than those on the pristine Ag (111) surface. In particular, the  $\text{Ag/Cs}_{22}\text{Cu}_{24}\text{Re}_{24}\text{Au}_{30}$  promoted Ag (111) surface may obtain the best selectivity for EO among various pristine and mixed-promoted Ag (111) surfaces considered. The following order of EO selectivity would be expected between the promoted and unpromoted Ag (111) surfaces:

$$\begin{aligned} \text{pristine Ag} &< \text{Ag/Cs-Mo} < \text{Ag/Cs}_{33,3}\text{Au}_{33,3}\text{Cu}_{33,3} < \text{Ag/Cs}_{25}\text{Cu}_{25}\text{Au}_{25}\text{Re}_{25} < \text{Ag/Cs-Cu} < \text{Ag/Cs-Zn} < \text{Ag/Cs-Au} \\ &< \text{Ag/Cs}_{33,3}\text{Re}_{33,3}\text{Au}_{33,3} < \text{Ag/Cs}_{22}\text{Rh}_{24}\text{Re}_{24}\text{Au}_{30} < \text{Ag/Cs-W} < \text{Ag/Cs}_{33,3}\text{Cu}_{33,3}\text{Re}_{33,3} < \text{Ag/Cs-Rh} < \text{Ag/Cs-Au} \\ &< \text{Ag/Cs-Re} < \text{Ag/Cs}_{22}\text{Cu}_{24}\text{Re}_{24}\text{Au}_{30} \end{aligned}$$

Figures 6 and 7 show that adding TM promoters can improve selectivity and activity, consistent with prior studies<sup>8,30,31,101</sup>. On an  $\text{Ag/Cs}_{22}\text{Cu}_{24}\text{Re}_{24}\text{Au}_{30}$  promoted Ag (111) surface, for instance,  $\Delta\Delta E_{Activation}$  increased from 1.29 to 2.71 eV compared to pristine Ag. A higher selectivity value indicates that the activation energy for acetaldehyde formation is greater than that for ethylene oxide formation. Consequently, the elevated activation energy (barrier energy) results in a slower formation rate of acetaldehyde compared to ethylene oxide. Compared with a Cs-promoted Ag (111) surface, the activation energy increased by only 0.69 eV, from 1.29 to 1.98 eV. Notably, Cu as a lone promoter may not positively affect EO selectivity. Consequently, Cu plays an important role when combined with other promoters to achieve high EO selectivity. Indeed, Cu improves the EO selectivity when combined with promoters such as Cs, Au, and Re, among others<sup>29,30</sup>.

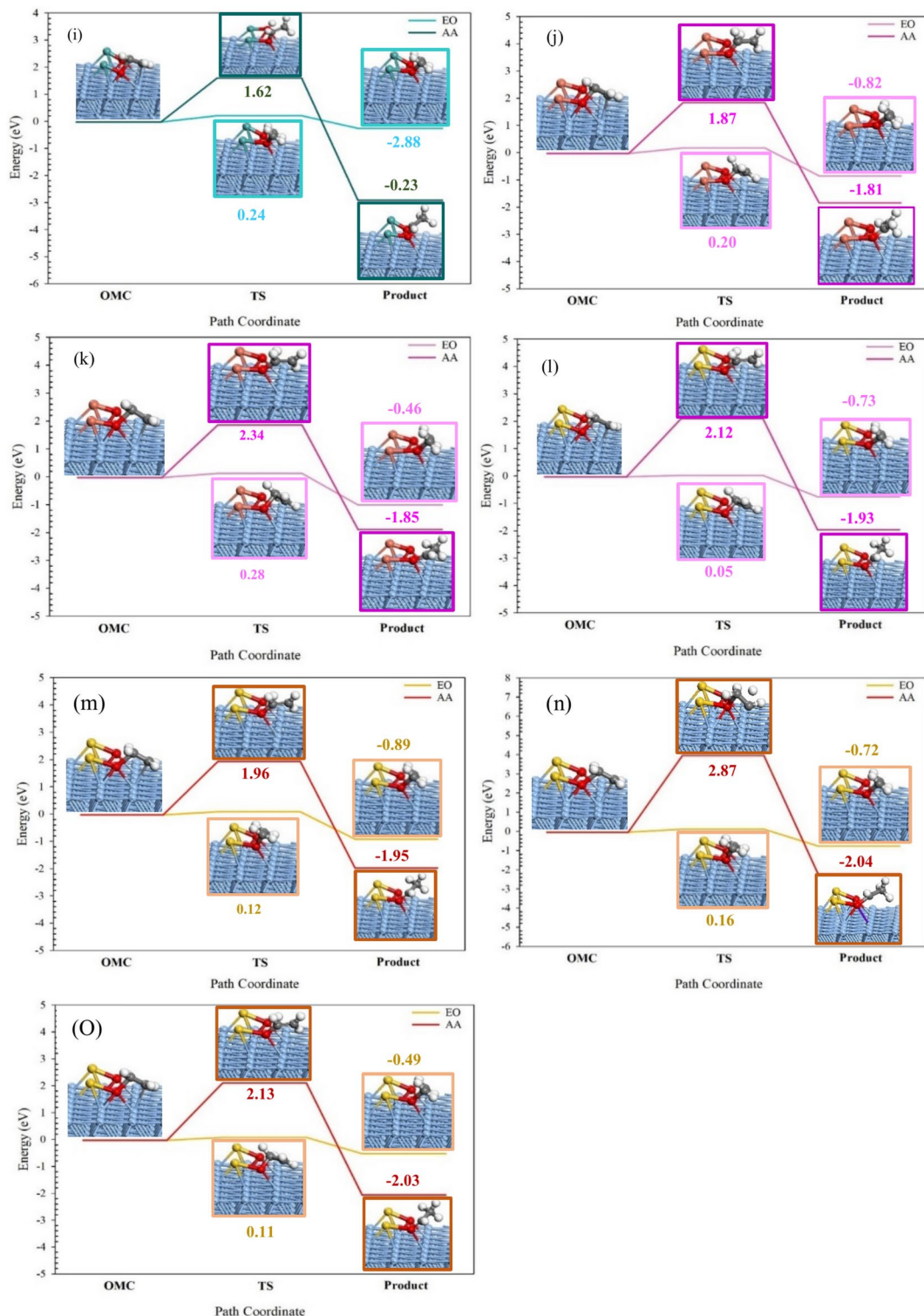
Our findings indicate that the mixed TM-promoted Ag (111) surface exhibits better EO selectivity and activity than the common Cs-promoted Ag surfaces. That would imply mixed TM catalysts can act efficiently



**Fig. 5.** Minimum-energy pathway of the Ethylene epoxidation reaction over (a) Ag, (b) Ag/Cs, (c) Ag/Cs-Rh, (d) Ag/Cs-Au, (e) Ag/Cs-Re, (f) Ag/Cs-Cu, (g) Ag/Cs-W, (h) Ag/Cs-Zn, (i) Ag/Cs-Mo, (j) Ag/Cs<sub>33.3</sub>Au<sub>33.3</sub>Cu<sub>33.3</sub>, (k) Ag/Cs<sub>33.3</sub>Re<sub>33.3</sub>Cu<sub>33.3</sub>, (l) Ag/Cs<sub>33.3</sub>Re<sub>33.3</sub>Au<sub>33.3</sub>, (m) Ag/Cs<sub>25</sub>Cu<sub>25</sub>Re<sub>25</sub>Au<sub>25</sub>, (n) Ag/Cs<sub>22</sub>Cu<sub>24</sub>Re<sub>24</sub>Au<sub>30</sub>, (o) Ag/Cs<sub>22</sub>Rh<sub>24</sub>Re<sub>24</sub>Au<sub>30</sub>, catalysts.

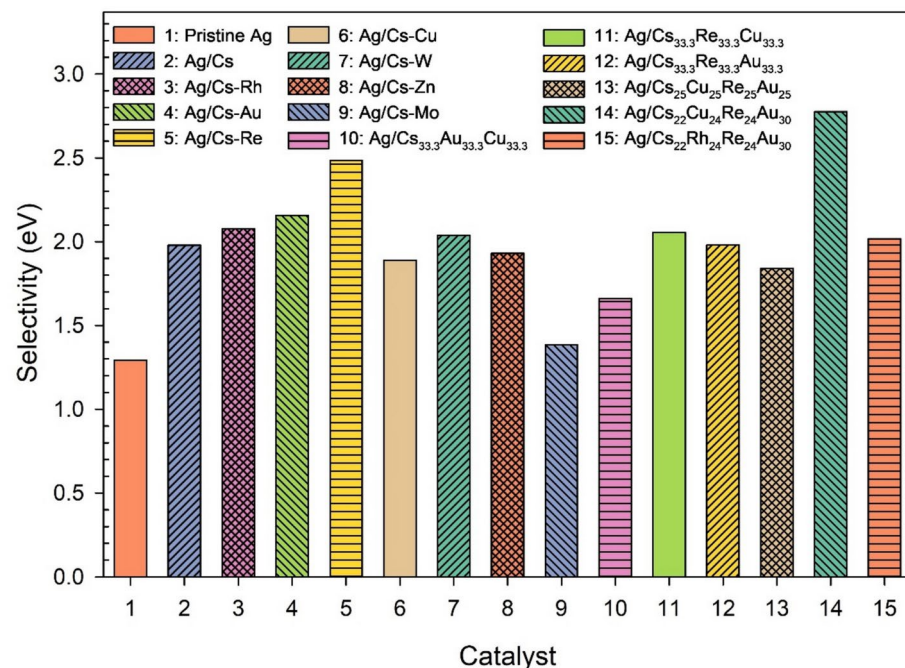
to catalyze the ethylene epoxidation reaction, such as Ag with Ag/Cs<sub>22</sub>Cu<sub>24</sub>Re<sub>24</sub>Au<sub>30</sub>, for better performance of ethylene oxide production.

It was found that highly active sites, such as those present on Ag (111), can significantly influence the overall reaction kinetics<sup>49</sup>. However, practically speaking, Ag catalysts can be affected by various factors, such

**Figure 5.** (continued)

as additional active sites and reaction conditions. Therefore, while the simulations in this study mainly focus on the intrinsic characteristics of different Ag facets under specific conditions, it is important to highlight that catalytic performance involves a combination of various facets, including Ag (111), Ag (100), Ag (110), as well as vacancies and defects. According to earlier investigations, Ag (111) surfaces show higher thermodynamic stability in comparison with both Ag(100) and Ag (110) surfaces. Such improved stability could slow down deactivation during reactions and longer catalyst lifetimes, rendering Ag (111) a preferred crystalline plane for a selective EO reaction. By contrast, Ag (100) and Ag (110) surfaces were characterized by lower stability and

Step	Reaction	Type
1	$O_{2(g)} + * \rightarrow O_2*$	Physisorption
2	$C_2H_{4(g)} + * \rightarrow C_2H_4*$	Physisorption
3*	$O_2 *_{(g)} + 2* \rightarrow 2O*$	Langmuir–Hinshelwood reaction
3	$O_{2(g)} + 2* \rightarrow 2O*$	Dissociative adsorption
4*	$C_2H_4 * + O * \rightleftharpoons OMC * + *$	Langmuir–Hinshelwood reaction
4	$C_2H_{4(g)} + O * \rightleftharpoons OMC*$	Eley–Rideal reaction
5	$OMC * \rightleftharpoons EO*$	Langmuir–Hinshelwood reaction
6	$OMC * \rightleftharpoons AA*$	Langmuir–Hinshelwood reaction
7	$EO * \rightleftharpoons EO + *$	Desorption
8	$AA * \rightleftharpoons AA + *$	Desorption

**Table 3.** List of elementary steps for partial and complete oxidation of ethylene on the developed catalysts<sup>12</sup>.**Fig. 6.** Comparison of ethylene oxide selectivity (in eV) obtained over the developed catalysts.

may undergo deactivation/reconstruction under certain reaction conditions, adversely affecting their efficiency. Indeed, while Ag (110) surfaces may show distinct reactivity patterns and high selectivity, their overall activity (e.g., longevity and stability) may not compete with that of Ag (111)<sup>82</sup>.

Moreover, the catalytic activity on the Ag (111) surfaces, especially when modified by the promoters, can be superior<sup>32,33</sup>. This is also due to the incorporation of promoters leading to improved adsorption of intermediates, which results in enhanced reaction rates.

## Conclusion

The DFT method has provided valuable insights into how Cs and various transition metal(s)—specifically Re, Rh, Au, Cu, W, Zn, and Mo—enhance the performance of silver catalysts in the ethylene epoxidation process. The adsorption strengths of the oxygen atom and ethylene on mixed-promoted Ag (111) surfaces were significantly higher than those on pristine Ag (111). The following outlines the order of selectivity for EO on both promoted and unpromoted Ag (111) surfaces:

pristine Ag < Ag/Cs-Mo < Ag/Cs<sub>33.3</sub>Au<sub>33.3</sub>Cu<sub>33.3</sub> < Ag/Cs<sub>25</sub>Cu<sub>25</sub>Re<sub>25</sub>Au<sub>25</sub> < Ag/Cs-Cu < Ag/Cs-Zn < Ag/Cs < Ag/Cs<sub>33.3</sub>Re<sub>33.3</sub>Au<sub>33.3</sub> < Ag/Cs<sub>22</sub>Rh<sub>24</sub>Re<sub>24</sub>Au<sub>30</sub> < Ag/Cs-W < Ag/Cs<sub>33.3</sub>Re<sub>33.3</sub> < Ag/Cs-Rh < Ag/Cs-Au < Ag/Cs-Re < Ag/Cs<sub>22</sub>Cu<sub>24</sub>Re<sub>24</sub>Au<sub>30</sub>.

Among the catalysts of Cs<sub>22</sub>Au<sub>24</sub>Cu<sub>24</sub>Re<sub>30</sub> promoted-Ag (111) and Cs<sub>22</sub>Au<sub>24</sub>Re<sub>30</sub> promoted-Ag (111), the highest EO selectivity and activity were found, respectively. The lowest selectivity and activity were found in unpromoted Ag (111). Such high EO selectivity achieved through co-promotion with TM(s) is attributed to specific structural interactions involving geometric and electronic factors. When electron-withdrawing TM(s)

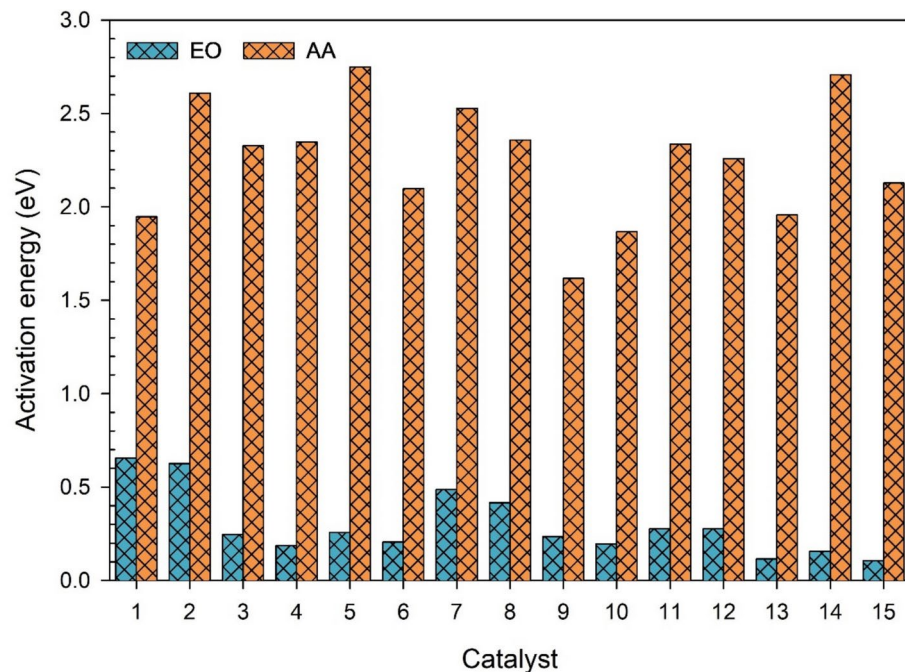


**Fig. 7.** Activation energy barriers (in eV) determine the activity for the epoxidation of ethylene on pristine or promoted Ag (111) catalysts. (1) Ag, (2) Ag/Cs, (3) Ag/Cs-Rh, (4) Ag/Cs-Au, (5) Ag/Cs-Re, (6) Ag/Cs-Cu, (7) Ag/Cs-W, (8) Ag/Cs-Zn, (9) Ag/Cs-Mo, (10) Ag/Cs<sub>33.3</sub>Au<sub>33.3</sub>Cu<sub>33.3</sub>, (11) Ag/Cs<sub>33.3</sub>Re<sub>33.3</sub>Cu<sub>33.3</sub>, (12) Ag/Cs<sub>33.3</sub>Re<sub>33.3</sub>Au<sub>33.3</sub>, (13) Ag/Cs<sub>25</sub>Cu<sub>25</sub>Re<sub>25</sub>Au<sub>25</sub>, (14) Ag/Cs<sub>22</sub>Cu<sub>24</sub>Re<sub>24</sub>Au<sub>30</sub>, (15) Ag/Cs<sub>22</sub>Rh<sub>24</sub>Re<sub>24</sub>Au<sub>30</sub>.

interact with electron-donating Cs, the charge transfer from the promoters to the catalyst is optimized. The effective combination of Cs and TM(s) helps prevent the Ag centers from becoming overly electrophilic, assisting in forming EO and nucleophilic O species while simultaneously suppressing ethylene combustion. The charge transferred by the promoters to the catalyst could be used to describe the EO selectivity. Further, this understanding of how TMs act as promoters towards Ag-based catalysts for ethylene epoxidation by the activation of atomic oxygen species would, in turn, enable future rational design of highly efficient Ag-based catalysts.

## Data availability

The datasets used and/or analyzed during the current study are available from the corresponding author upon reasonable request.

Received: 29 November 2024; Accepted: 24 March 2025

Published online: 17 April 2025

## References

- Lohr, T. L. et al. Ethylene oxide: A catalyst and process development success story. *Ind. Eng. Chem. Res.* **63**(43), 18221–18240 (2024).
- Jones, T. E. et al. The selective species in ethylene epoxidation on silver. *ACS Catal.* **8**, 3844–3852 (2018).
- Jones, T. E. et al. Oxidation of ethylene on oxygen reconstructed silver surfaces. *J. Phys. Chem. C* **120**, 28630–28638 (2016).
- Kestenbaum, H. et al. Silver-catalyzed oxidation of ethylene to ethylene oxide in a microreaction system. *Ind. Eng. Chem. Res.* **41**, 710–719 (2002).
- Impeng, S. et al. High selective catalyst for ethylene epoxidation to ethylene oxide: A DFT investigation. *Appl. Surf. Sci.* **513**, 145799 (2020).
- Kim, Y.-C. et al. Partial oxidation of ethylene to ethylene oxide over nanosized Ag/α-Al<sub>2</sub>O<sub>3</sub> catalysts. *Catal. Today* **87**, 153–162 (2003).
- Burch, R., Squire, G. D. & Tsang, S. C. Role of chlorine in improving selectivity in the oxidative coupling of methane to ethylene. *Appl. Catal.* **46**, 69–87 (1989).
- Jankowiak, J. T. & Barreau, M. A. Ethylene epoxidation over silver and copper–silver bimetallic catalysts: II. Cs and Cl promotion. *J. Catal.* **236**, 379–386 (2005).
- Scharfenberg, L. & Horn, R. Temporal analysis of products experiments at atmospheric pressure: The epoxidation of ethylene on silver. *Chem. Ing. Tec.* **89**, 1350–1359 (2017).
- Andryushechkin, B. V., Shevlyuga, V. M., Pavlova, T. V., Zhidomirov, G. M. & Eltsov, K. N. Adsorption of molecular oxygen on the Ag (111) surface: A combined temperature-programmed desorption and scanning tunneling microscopy study. *J. Chem. Phys.* **148**, 244702 (2018).
- Aho, A. et al. Ethylene epoxidation over supported silver catalysts—Influence of catalyst pretreatment on conversion and selectivity. *J. Chem. Technol. Biotechnol.* **93**, 1549–1557 (2018).
- Huš, M., Grilc, M., Pavlišić, A., Likozar, B. & Hellman, A. Multiscale modelling from quantum level to reactor scale: An example of ethylene epoxidation on silver catalysts. *Catal. Today* **338**, 128–140 (2019).

13. Chen, B. W. J., Wang, B., Sullivan, M. B., Borgna, A. & Zhang, J. Unraveling the synergistic effect of Re and Cs promoters on ethylene epoxidation over silver catalysts with machine learning-accelerated first-principles simulations. *ACS Catal.* **12**, 2540–2551 (2022).
14. Xu, H., Zhu, L., Nan, Y., Xie, Y. & Cheng, D. Revisit the Role of metal dopants in enhancing the selectivity of Ag-catalyzed ethylene epoxidation: Optimizing oxophilicity of reaction site via cocatalytic mechanism. *ACS Catal.* **11**, 3371–3383 (2021).
15. Jones, T. E. et al. Thermodynamic and spectroscopic properties of oxygen on silver under an oxygen atmosphere. *Phys. Chem. Chem. Phys.* **17**, 9288–9312 (2015).
16. Derouin, J., Farber, R. G., Turano, M. E., Iski, E. V. & Killelea, D. R. Thermally selective formation of subsurface oxygen in Ag (111) and consequent surface structure. *ACS Catal.* **6**, 4640–4646 (2016).
17. Heine, C., Eren, B., Lechner, B. A. J. & Salmeron, M. A study of the O/Ag (111) system with scanning tunneling microscopy and x-ray photoelectron spectroscopy at ambient pressures. *Surf. Sci.* **652**, 51–57 (2016).
18. Ashkhотов, О. Г., Кхубезхов, С. А., Алерев, М. А., Магкоеv, Т. Т. & Григоркина, Г. С. Effect of bombardment with oxygen ions on the surface composition of polycrystalline silver. *Russ. J. Phys. Chem. A* **92**, 1382–1385 (2018).
19. Salaev, M. A., Salaeva, A. A. & Vodyankina, O. V. Towards the understanding of promoting effects of Re, Cs and Cl promoters for silver catalysts of ethylene epoxidation: A computational study. *Catal. Today* **375**, 585–590 (2021).
20. Wyrwich, R. et al. LEED-I (V) structure analysis of the  $(7\sqrt{3}\times 3)$  rect SO<sub>4</sub> phase on Ag (111): Precursor to the active species of the Ag-catalyzed ethylene epoxidation. *J. Phys. Chem. C* **122**, 26998–27004 (2018).
21. Saravanan, C., Salazar, M. R., Kress, J. D. & Redondo, A. Oxametallacycle intermediates on clean and Cs-promoted Ag (111) surfaces. *J. Phys. Chem. B* **104**, 8685–8691 (2000).
22. Linic, S. & Barreau, M. A. On the mechanism of Cs promotion in ethylene epoxidation on Ag. *J. Am. Chem. Soc.* **126**, 8086–8087 (2004).
23. Ren, D., Xu, H., Li, J., Li, J. & Cheng, D. Origin of enhanced ethylene oxide selectivity by Cs-promoted silver catalyst. *Mol. Catal.* **441**, 92–99 (2017).
24. Machocki, A. et al. Manganese–lanthanum oxides modified with silver for the catalytic combustion of methane. *J. Catal.* **227**, 282–296 (2004).
25. Stegelmann, C., Schiødt, N. C., Campbell, C. T. & Stoltze, P. Microkinetic modeling of ethylene oxidation over silver. *J. Catal.* **221**, 630–649 (2004).
26. Kokalj, A., Gava, P., de Gironcoli, S. & Baroni, S. What determines the catalyst's selectivity in the ethylene epoxidation reaction. *J. Catal.* **254**, 304–309 (2008).
27. Jingfa, D., Jun, Y., Shi, Z. & Xiaohong, Y. Promoting effects of Re and Cs on silver catalyst in ethylene epoxidation. *J. Catal.* **138**(1), 395–399 (1992).
28. Ren, D. et al. Effect of rhenium loading sequence on selectivity of Ag–Cs catalyst for ethylene epoxidation. *Catal. Lett.* **147**, 2920–2928 (2017).
29. Zhu, L. et al. The synergistic effect between crystal planes and promoters on Ag-catalyzed ethylene epoxidation. *Appl. Surf. Sci.* **476**, 115–122 (2019).
30. Diao, W., DiGiulio, C. D., Schaal, M. T., Ma, S. & Monnier, J. R. An investigation on the role of Re as a promoter in AgCsRe/α-Al<sub>2</sub>O<sub>3</sub> high-selectivity, ethylene epoxidation catalysts. *J. Catal.* **322**, 14–23 (2015).
31. Dellamorte, J. C., Lauterbach, J. & Barreau, M. A. Rhenium promotion of Ag and Cu–Ag bimetallic catalysts for ethylene epoxidation. *Catal. Today* **120**, 182–185 (2007).
32. Dellamorte, J. C., Lauterbach, J. & Barreau, M. A. Promoter-induced morphological changes of Ag catalysts for ethylene epoxidation. *Ind. Eng. Chem. Res.* **48**, 5943–5953 (2009).
33. Li, Z., Zhu, L., Chen, J.-F. & Cheng, D. Enhanced ethylene oxide selectivity by Cu and Re dual-promoted Ag catalysts. *Ind. Eng. Chem. Res.* **57**, 4180–4185 (2018).
34. Özbek, M. O., Önal, I. & van Santen, R. A. Chlorine and caesium promotion of silver ethylene epoxidation catalysts. *ChemCatChem* **5**, 443–451 (2013).
35. Chen, H.-T., Chang, J.-G., Ju, S.-P. & Chen, H.-L. Ethylene epoxidation on a Au nanoparticle versus a Au (111) surface: A DFT study. *J. Phys. Chem. Lett.* **1**, 739–742 (2010).
36. Lee, C.-C. & Chen, H.-T. Adsorption and reaction of C<sub>2</sub>H<sub>4</sub> and O<sub>2</sub> on a Nanosized gold cluster: A computational study. *J. Phys. Chem. A* **119**, 8547–8555 (2015).
37. Hwang, A., Klaucke, J., Lizandara-Pueyo, C., Karpov, A. & Iglesia, E. Roles of Re and Cs promoters and organochlorine moderators in the synthesis of ethylene oxide on Ag-based catalysts. *ChemCatChem* **16**, e202301369 (2024).
38. Salaev, M. A. Computational insights into promoting effects of alkali metals, Re, and Cl for silver catalysts of ethylene epoxidation. *Mol. Catal.* **507**, 111574 (2021).
39. Giannozzi, P. et al. QUANTUM ESPRESSO: A modular and open-source software project for quantum simulations of materials. *J. Phys.: Condens. Matter* **21**, 395502 (2009).
40. Grimme, S. Semiempirical GGA-type density functional constructed with a long-range dispersion correction. *J. Comput. Chem.* **27**, 1787–1799 (2006).
41. Bende, D., Wagner, F. R., Sichevych, O. & Grin, Y. Chemical bonding analysis as a guide for the preparation of new compounds: The case of VIrGe and HfPtGe. *Angew. Chem.* **129**, 1333–1338 (2017).
42. Henkelman, G., Überuaga, B. P. & Jónsson, H. A climbing image nudged elastic band method for finding saddle points and minimum energy paths. *J. Chem. Phys.* **113**, 9901–9904 (2000).
43. Clark, S. J. et al. First principles methods using CASTEP. *Zeitschrift für Kristallographie Crystalline Materials.* **220**, 567–570 (2005).
44. Wu, S., Tatarchuk, B. J. & Adamczyk, A. J. Ethylene oxidation on unpromoted silver catalysts: Reaction pathway and selectivity analysis using DFT calculations. *Surf. Sci.* **708**, 121834 (2021).
45. Pu, T. et al. Nature and reactivity of oxygen species on/in silver catalysts during ethylene oxidation. *ACS Catal.* **12**, 4375–4381 (2022).
46. Liu, C. et al. Computational and experimental insights into reactive forms of oxygen species on dynamic Ag surfaces under ethylene epoxidation conditions. *J. Catal.* **405**, 445–461 (2022).
47. Hayat, S. S., Ortigoza, M. A., Choudhry, M. A. & Rahman, T. S. Diffusion of the Cu monomer and dimer on Ag (111): Molecular dynamics simulations and density functional theory calculations. *Phys. Rev. B* **82**, 85405 (2010).
48. Li, W.-X., Stampfl, C. & Scheffler, M. Oxygen adsorption on Ag (111): A density-functional theory investigation. *Phys. Rev. B* **65**, 75407 (2002).
49. Pu, T., Tian, H., Ford, M. E., Rangarajan, S. & Wachs, I. E. Overview of selective oxidation of ethylene to ethylene oxide by Ag catalysts. *ACS Catal.* **9**, 10727–10750 (2019).
50. Podgornov, E. A., Prosvirin, I. P. & Bukhtiyarov, V. I. XPS, TPD and TPR studies of Cs–O complexes on silver: Their role in ethylene epoxidation. *J. Mol. Catal. A: Chem.* **158**, 337–343 (2000).
51. Bal'zhinimae, B. S. Ethylene epoxidation over silver catalysts. *Kinet. Catal.* **40**, 795–810 (1999).
52. Liu, X., Guo, H. & Meng, C. Oxygen adsorption and diffusion on NiTi alloy (100) surface: A theoretical study. *The Journal of Physical Chemistry C* **116**, 21771–21779 (2012).
53. Jones, T. E. et al. Insights into the electronic structure of the oxygen species active in alkene epoxidation on silver. *ACS Catal.* **5**, 5846–5850 (2015).

54. Keivaniemehr, F. et al. Electrocatalytic hydrogen evolution on the noble metal-free MoS<sub>2</sub>/carbon nanotube heterostructure: A theoretical study. *Sci. Rep.* **11**, 1–9 (2021).
55. Alavijeh, M. M. et al. A selective and efficient precious metal-free electrocatalyst for chlorine evolution reaction: An experimental and computational study. *Chem. Eng. J.* **421**, 127785 (2021).
56. Kaichev, V. V. et al. The nature of electrophilic and nucleophilic oxygen adsorbed on silver. *Kinet. Catal.* **44**, 432–440 (2003).
57. Bukhtiyarov, V. I. et al. Combined application of XANES and XPS to study oxygen species adsorbed on Ag foil. *Nucl. Instrum. Methods Phys. Res., Sect. A* **470**, 302–305 (2001).
58. Bukhtiyarov, V. I. et al. Atomic oxygen species on silver: Photoelectron spectroscopy and x-ray absorption studies. *Phys. Rev. B* **67**, 235422 (2003).
59. Choudhuri, D. et al. Exceptional increase in the creep life of magnesium rare-earth alloys due to localized bond stiffening. *Nat. Commun.* **8**, 1–9 (2017).
60. Jiang, C. & Srinivasan, S. G. Unexpected strain-stiffening in crystalline solids. *Nature* **496**, 339–342 (2013).
61. Huš, M. & Hellman, A. Dipole effect on ethylene epoxidation: Influence of alkali metals and chlorine. *J. Catal.* **363**, 18–25 (2018).
62. Kilty, P. A. & Sachtler, W. M. H. The mechanism of the selective oxidation of ethylene to ethylene oxide. *Catal. Rev.: Sci. Eng.* **10**, 1–16 (1974).
63. Zhu, L., Zhang, W., Zhu, J. & Cheng, D. Mechanistic insight into the facet-dependent selectivity of ethylene epoxidation on Ag nanocatalysts. *Appl. Catal. A Gen.* **538**, 27–36 (2017).
64. Reuter, K. & Scheffler, M. Composition and structure of the RuO<sub>2</sub>(110) surface in an O<sub>2</sub> and CO environment: Implications for the catalytic formation of CO<sub>2</sub>. *Phys. Rev. B* **68**, 45407 (2003).
65. Kiejna, A. et al. Comparison of the full-potential and frozen-core approximation approaches to density-functional calculations of surfaces. *Phys. Rev. B* **73**, 35404 (2006).
66. Wang, H. & Schneider, W. F. Effects of coverage on the structures, energetics, and electronics of oxygen adsorption on RuO<sub>2</sub>(110). *J. Chem. Phys.* **127**, 64706 (2007).
67. Yu, Y. et al. Dissociative adsorption of O<sub>2</sub> on Ag<sub>3</sub>Au(111) surface: A density functional theory study. *Crystals Basel* **14**, 504 (2024).
68. Boronat, M., Pulido, A., Concepción, P. & Corma, A. Propene epoxidation with O<sub>2</sub> or H<sub>2</sub>-O<sub>2</sub> mixtures over silver catalysts: Theoretical insights into the role of the particle size. *Phys. Chem. Chem. Phys.* **16**, 26600–26612 (2014).
69. Dutta, S., Indra, A., Feng, Y., Han, H. & Song, T. Promoting electrocatalytic overall water splitting with nanohybrid of transition metal nitride-oxynitride. *Appl. Catal. B* **241**, 521–527 (2019).
70. Cheng, X. et al. NO reduction by CO over copper catalyst supported on mixed CeO<sub>2</sub> and Fe<sub>2</sub>O<sub>3</sub>: Catalyst design and activity test. *Appl. Catal. B* **239**, 485–501 (2018).
71. Reddy, B. M., Rao, K. N. & Bharali, P. Copper promoted cobalt and nickel catalysts supported on ceria–alumina mixed oxide: Structural characterization and CO oxidation activity. *Ind. Eng. Chem. Res.* **48**, 8478–8486 (2009).
72. Keivaniemehr, F., Habibzadeh, S. & Mokhtarian, M. Enhanced product quality through hydrodesulfurization of pyrolysis gasoline over a mixed metal oxide catalyst: An experimental and DFT study. *Fuel* **317**, 123458 (2022).
73. Linic, S., Medlin, J. W. & Barteau, M. A. Synthesis of oxametallacycles from 2-iodoethanol on Ag(111) and the structure dependence of their reactivity. *Langmuir* **18**, 5197–5204 (2002).
74. Linic, S. & Barteau, M. A. Construction of a reaction coordinate and a microkinetic model for ethylene epoxidation on silver from DFT calculations and surface science experiments. *J. Catal.* **214**, 200–212 (2003).
75. Bocquet, M.-L. & Loffreda, D. Ethene epoxidation selectivity inhibited by twisted oxametallacycle: A DFT study on Ag surface-oxide. *J. Am. Chem. Soc.* **127**, 17207–17215 (2005).
76. Li, M.-J. et al. The remarkable activity and stability of a highly dispersive beta-brass Cu-Zn catalyst for the production of ethylene glycol. *Sci. Rep.* **6**, 1–8 (2016).
77. Kim, Y. D. et al. Characterization of various oxygen species on an oxide surface: RuO<sub>2</sub>(110). *J. Phys. Chem. B* **105**, 3752–3758 (2001).
78. Paulus, U. A., Wang, Y., Bonzel, H. P., Jacobi, K. & Ertl, G. Adsorption and interaction of ethylene on RuO<sub>2</sub>(110) surfaces. *J. Phys. Chem. B* **109**, 2139–2148 (2005).
79. Gao, W., Zhao, M. & Jiang, Q. A DFT study on electronic structures and catalysis of Ag<sub>12</sub>O<sub>6</sub>/Ag(111) for ethylene epoxidation. *J. Phys. Chem. C* **111**, 4042–4046 (2007).
80. Torres, D. & Illas, F. On the performance of Au(111) for ethylene epoxidation: A density functional study. *J. Phys. Chem. B* **110**, 13310–13313 (2006).
81. Liu, X. et al. Defect stabilized gold atoms on graphene as potential catalysts for ethylene epoxidation: A first-principles investigation. *Catal. Sci. Technol.* **6**, 1632–1641 (2016).
82. Huš, M. & Hellman, A. Ethylene epoxidation on ag(100), ag(110), and ag(111): a joint ab initio and kinetic monte carlo study and comparison with experiments. *ACS Catal.* **9**, 1183–1196 (2018).
83. Jankowiak, J. T. & Barteau, M. A. Ethylene epoxidation over silver and copper–silver bimetallic catalysts: I. Kinetics and selectivity. *J. Catal.* **236**, 366–378 (2005).
84. Grant, R. B. & Lambert, R. M. Ethylene oxide isomerisation on single-crystal Ag(111) in atomically clean and Cs-moderated conditions. *J. Catal.* **93**, 92–99 (1985).
85. Verma, A. & Kaliaguine, S. Estimation of rate coefficients from pulsed microcatalytic reactors: Oxidation of ethylene over silver catalyst. *J. Catal.* **30**, 430–437 (1973).
86. Force, E. L. & Bell, A. T. The relationship of adsorbed species observed by infrared spectroscopy to the mechanism of ethylene oxidation over silver. *J. Catal.* **40**, 356–371 (1975).
87. Li, H. et al. Analysis of the limitations in the oxygen reduction activity of transition metal oxide surfaces. *Nat. Catal.* **4**, 463–468 (2021).
88. Li, H. & Nørskov, J. K. Effects of a conductive support on the bonding of oxygen containing molecules to transition metal oxide surfaces. *Phys. Chem. Chem. Phys.* **22**, 26216–26222 (2020).
89. Li, W.-X., Stampfl, C. & Scheffler, M. Why is a noble metal catalytically active? The role of the O-Ag interaction in the function of silver as an oxidation catalyst. *Phys. Rev. Lett.* **90**, 256102 (2003).
90. Guo, X.-C. & Madix, R. J. Adsorption of oxygen and carbon dioxide on cesium-reconstructed Ag(110) surface. *Surf. Sci.* **550**, 81–92 (2004).
91. Shi, H. & Stampfl, C. First-principles investigations of the structure and stability of oxygen adsorption and surface oxide formation at Au(111). *Phys. Rev. B* **76**, 75327 (2007).
92. Shumbera, R. B., Kan, H. H. & Weaver, J. F. Oxidation of Pt(100)-hex-R0.7 by gas-phase oxygen atoms. *Surf. Sci.* **601**, 235–246 (2007).
93. Soon, A., Todorova, M., Delley, B. & Stampfl, C. Surface oxides of the oxygen–copper system: Precursors to the bulk oxide phase?. *Surf. Sci.* **601**, 5809–5813 (2007).
94. Klikovits, J. et al. Surface oxides on Pd(111): STM and density functional calculations. *Phys. Rev. B* **76**, 45405 (2007).
95. Zhang, H., Soon, A., Delley, B. & Stampfl, C. Stability, structure, and electronic properties of chemisorbed oxygen and thin surface oxides on Ir(111). *Phys. Rev. B* **78**, 45436 (2008).
96. Zhang, W.-B. & Tang, B.-Y. Surface adsorption phase diagram of O/Ni(110) system: An ab initio atomistic thermodynamics investigation. *Appl. Phys. Lett.* **94**, 91901 (2009).

97. Stampfl, C. Surface processes and phase transitions from ab initio atomistic thermodynamics and statistical mechanics. *Catal. Today* **105**, 17–35 (2005).
98. Gustafson, J. et al. Self-limited growth of a thin oxide layer on Rh (111). *Phys. Rev. Lett.* **92**, 126102 (2004).
99. Campbell, C. T. The selective epoxidation of ethylene catalyzed by Ag (111): A comparison with Ag (110). *J. Catal.* **94**, 436–444 (1985).
100. Campbell, C. T. & Paffett, M. T. The role of chlorine promoters in catalytic ethylene epoxidation over the Ag (110) surface. *Applications of Surface Science* **19**, 28–42 (1984).
101. de Carvalho, M. C. N. A., Passos, E. B. & Schmal, M. Study of the active phase of silver catalysts for ethylene epoxidation. *J. Catal.* **248**, 124–129 (2007).

## Author contributions

All authors collaborated in writing, software developing, conception, data gathering, and resources.

## Declarations

### Competing interest

The authors declare no competing interests.

### Additional information

**Supplementary Information** The online version contains supplementary material available at <https://doi.org/10.1038/s41598-025-95642-2>.

**Correspondence** and requests for materials should be addressed to S.H.

**Reprints and permissions information** is available at [www.nature.com/reprints](http://www.nature.com/reprints).

**Publisher's note** Springer Nature remains neutral with regard to jurisdictional claims in published maps and institutional affiliations.

**Open Access** This article is licensed under a Creative Commons Attribution-NonCommercial-NoDerivatives 4.0 International License, which permits any non-commercial use, sharing, distribution and reproduction in any medium or format, as long as you give appropriate credit to the original author(s) and the source, provide a link to the Creative Commons licence, and indicate if you modified the licensed material. You do not have permission under this licence to share adapted material derived from this article or parts of it. The images or other third party material in this article are included in the article's Creative Commons licence, unless indicated otherwise in a credit line to the material. If material is not included in the article's Creative Commons licence and your intended use is not permitted by statutory regulation or exceeds the permitted use, you will need to obtain permission directly from the copyright holder. To view a copy of this licence, visit <http://creativecommons.org/licenses/by-nc-nd/4.0/>.

© The Author(s) 2025